J Low Temp Phys (2018) 190:1–19
https://doi.org/10.1007/s10909-017-1828-5

Entropy Constraints in the Ground State Formation of Magnetically Frustrated Systems

Role of Nernst Postulate in Real Systems

Julian G. Sereni[1]

Received: 13 June 2017 / Accepted: 20 October 2017 / Published online: 1 November 2017

Abstract A systematic modification of the entropy trajectory ($S_m(T)$) is observed at very low temperature in magnetically frustrated systems as a consequence of the constraint ($S_m \geq 0$) imposed by the Nernst postulate. The lack of magnetic order allows to explore and compare new thermodynamic properties by tracing the specific heat (C_m) behavior down to the sub-Kelvin range. Some of the most relevant findings are: (i) a common $C_m/T|_{T\to 0} \approx 7\,\mathrm{J/mol\,K^2}$ 'plateau' in at least five Yb-based very-heavy-fermions (VHF) compounds; (ii) quantitative and qualitative differences between VHF and standard non-Fermi-liquids; (iii) entropy bottlenecks governing the change of $S_m(T)$ trajectories in a continuous transition into alternative ground states. A comparative analysis of $S_m(T \to 0)$ dependencies is performed in compounds suitable for adiabatic demagnetization processes according to their $\partial^2 S_m/\partial T^2$ derivatives.

Keywords Entropy · Magnetic frustration · Specific heat · Heavy fermions · Ce and Yb compounds

1 Introduction

The intensive study of the quantum critical (QC) behavior in heavy fermion (HF) compounds [1,2] has powered the investigation of thermodynamic properties in a significant number of new Ce- and Yb-based intermetallics within the sub-Kelvin range of temperature. Despite the unattainability of the $T = 0$ limit, the extremely low characteristic energies of these systems provide a fertile field to allow to perform an empirical test for the applicability of the third law of thermodynamics on real

✉ Julian G. Sereni
jsereni@cab.cnea.gov.ar

[1] Low Temperature Division, CAB-CNEA and CONICET, 8400 San Carlos de Bariloche, Argentina

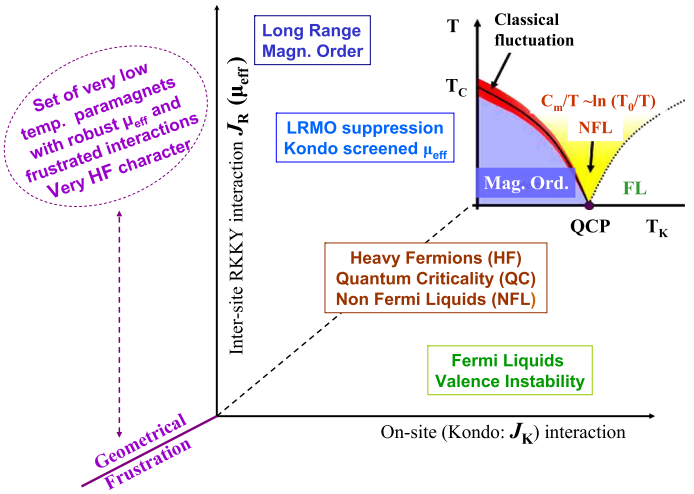

Fig. 1 Schematic description of the magnetic behavior of Ce- (Yb-) lattice compounds as a function of two exchange parameters (see the text). The third axis represents frustrated (paramagnetic) systems. Inset: usual representation as a function of Kondo temperature [5–7] (Color figure online)

systems. As a consequence of this newly available information, unexplored behaviors of the thermal dependence of the entropy (S_m) have emerged within the thermal range where thermodynamic and QC fluctuations interplay to stabilize the ground states of not ordered systems because "geometric frustration implies relatively strong quantum fluctuation…" [3]. More recently, a renewed interest on the low temperature $S_m(T)$ trajectory arose in the search of cryo-materials suitable for adiabatic demagnetization refrigeration within the mK range [4]. Within the general scope of this work is the analysis of that thermodynamic parameter in Ce and Yb compounds that show very large density of excitations approaching zero temperature.

The usual magnetic behavior of Ce- and Yb-based intermetallics can be properly described as a function of two coupling parameters [5–7]: the inter-site RKKY magnetic interaction (J_R) and the on-site Kondo (J_K) interaction. As the local J_K coupling between band and localized $4f$ states increases, the intensity of the magnetic moments (μ_{eff}) decreases because of the so-called Kondo screening. The consequent weakening of J_R ($\propto \mu_{eff}$) is reflected in the decrease of the magnetic order temperature (T_{ord}) that can be driven down to a QC-point at $T \rightarrow 0$ [8]. The different stages of this demagnetizing process as a function of J_K is schematically resumed in Fig. 1.

Once T_{ord} reaches the range at which quantum and thermal fluctuations compete in energy, the QC scenario sets on [1,2]. This regime is observed in heavy fermion (HF) compounds which behave as non-fermi-liquids (NFL) while they approach the QCP (see the inset in Fig. 1). Once J_K overcomes J_R the Fermi Liquid (FL) behavior takes over. Within this regime the thermal ($\gamma = C_m/T$), magnetic (χ_0) and transport ($\rho = AT^2$) proportionality: $\gamma \propto \chi_0 \propto \sqrt{A} \propto m_{eff}$ is fulfilled, m_{eff} being the enhanced effective electron mass.

There is, however, an increasing set of Ce and Yb compounds which escape from this description because they do not order magnetically despite their robust μ_{eff} (i.e.,

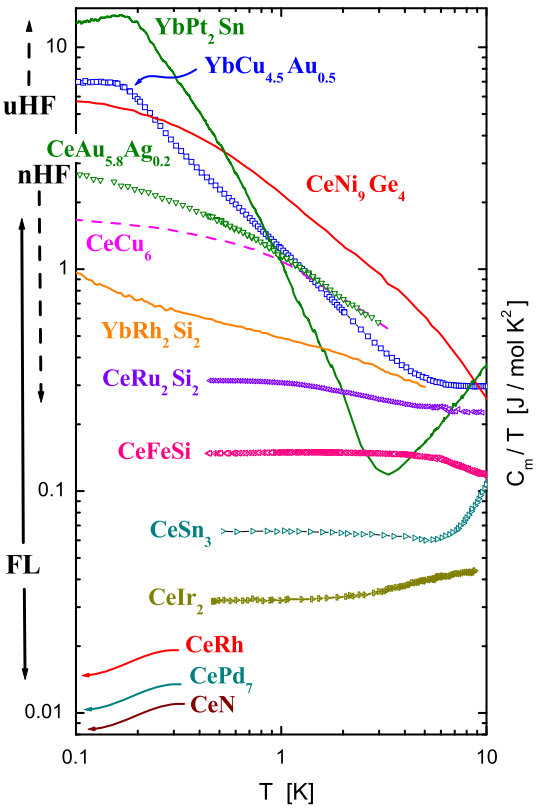

Fig. 2 Examples of measured $C_m/T|_{T\to 0}$ values within four decades, identifying three groups according their different behaviors: Fermi liquids (FL), 'normal heavy fermions (nHF) and upper heavy fermions (uHF), see the text. For binary FL, see references in [9] and for ternary compounds see [10–13] (Color figure online)

$J_R \gg J_K$) in a lattice arrangement. This behavior may arise from frustrated interactions between magnetic neighbors favored by some types of atomic coordinations. Alternatively, the lack of magnetic order may also be due to a weakened $J_R \propto 1/d^3$ interaction by a large interatomic spacing (d) between magnetic moments. This peculiar group is included in the expanded phase diagram presented in Fig. 1 by introducing a third axis.

2 Different Classes of Heavy Fermions

Among the Ce and Yb compounds which do not order magnetically, the measured values of specific heat at $T \to 0$ ($C_m/T|_{T\to 0}$) cover more than three decades between the lowest reported value $\approx 8\,\mathrm{mJ/mol\,K^2}$ in CeN and $CePd_7$ [9] and the highest $\approx 12\,\mathrm{J/mol\,K^2}$ observed in $YbPt_2Sn$ [11], see Fig. 2. CeN and $CePd_7$ are characterized by a strong local ($4f$) and conduction states hybridization ($\propto J_K$) reflected in a large Kondo temperature, $T_K \propto \exp(-1/J_K)$ [5–7].

On the weak hybridization range, the exemplary FL-HF with the highest $C_m/T|_{T\to 0}$ is $CeCu_6$ with a $\gamma = 1.6\,\mathrm{J/mol\,K^2}$ [13] and $T_K \approx 10\,\mathrm{K}$. Its FL character is proved by the low temperature $\rho = AT^2$ dependence. Between $1 \le C_m/T|_{T\to 0} \le 3\,\mathrm{J/mol\,K^2}$

the most frequently observed behavior corresponds to compounds showing the characteristic NFL dependence: $C_m/T \propto -\ln(T/T_0)$ [1], where the energy scale T_0 plays a similar role than T_K. Coincidentally, the most representative NFL compounds show a $\rho \propto T$ dependence [14].

Recently, some Ce and a significant number of Yb compounds were found to clearly exceed the $C_m/T|_{T\to 0}$ values of NFL. These compounds are identified as upper-HF (uHF) because their $C_m/T|_{T\to 0}$ range between ≈ 5 and $\approx 12\,\mathrm{J/mol\,K^2}$, see the compounds lying in the 'upper' part of Fig. 2 in contrast of the normal-HF (nHF). The absence of magnetic order in these systems coincides with a huge increase of their spin correlations (SC) in the paramagnetic (PM) phase by cooling. Since at that range of temperature their magnetic behavior does not fit into the typical Curie-Weiss paramagnetism for single magnetic moments, hereafter they will be identified as 'SC-PM'. The strong increase of the density of magnetic excitations is reflected in a divergent power law dependence of $C_m(T)/T \propto 1/T^Q$, with exponents ranging between $1 \leq Q \leq 2$. This behavior is observed down to a characteristic temperature (T_{BN}) below which a clear deviation from the SC-PM behavior occurs due to an entropy-bottleneck (BN) formation.

Apart from the different values of $C_m/T|_{T\to 0}$ between NFL-HF and uHF, there are other distinctive properties indicating that these materials belong to different classes. An intrinsic difference is that NFL are located in the QC region, as depicted in the inset of Fig. 1. On the contrary, uHF exhibit robust moments with irrelevant Kondo effect, being the geometrical frustration responsible for the lack of magnetic order, with different thermal dependencies. While the $C_m(T)/T \propto -\ln(T/T_0)$ dependence of NFL was found to scale different compounds through their T_0 temperatures [15], see Fig. 3a, the scaling among uHF compounds occurs through the exponents Q of their $1/T^Q$ dependencies. This feature is presented in Fig. 3b for five Yb-based examples using the following values: $Q = 1.1 \pm 0.2$ for $YbCu_{5-x}Au_x$ ($0.4 \leq x \leq 0.7$) [12], $Q = 1.2$ for $YbCu_4Ni$ [16] and $Q = 1.4$ for $PrInAg_2$ [17]. Notably, all these compounds show a nearly coincident $C_m/T|_{T\to 0} \approx 7 \pm 0.7\,\mathrm{J/mol\,K^2}$ 'plateau' below their respective characteristic temperatures T_{BN}.

There are other two compounds belonging to this uHF group: YbBiPt [18] and $YbCo_2Zn_{20}$ [19]. Although they show the same $C_m/T|_{T\to 0}$ values, they are not included in Fig. 3b because their low-energy crystal electric field (CEF) levels already contribute to $C_m(T)/T$ around 1 K with the consequent deviation from the $1/T^Q$ dependence in the SC-PM phase. Except these two cases, all the compounds analyzed in this work own a well-defined doublet GS. Notably, the recently studied Sc-doped $YbCo_2Zn_{20}$ [20] system also fits into the NFL scaling presented in Fig. 3a for 19% of Sc content, with the record low value of $T_0 = 1.2$ K, whereas the low temperature contribution of the first excited CEF doublet is reflected in the large $\gamma_{HT} = 1.1\,\mathrm{J/mol\,K^2}$ term. This supports the vicinity of the parent compound $YbCo_2Zn_{20}$ to a QC-point as stated in Ref. [20].

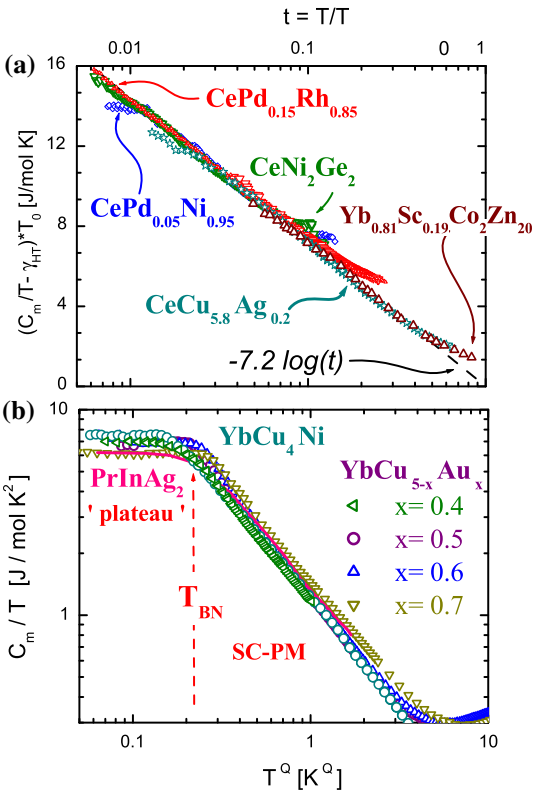

Fig. 3 **a** Overlap of $C_{\mathrm{m}}(t)$ dependencies of NFL-HF as a function of $-\ln(t)$ using a normalized temperature $t = T/T_0$ [15], where γ_{HT} accounts for the high temperature C_{m}/T contribution. **b** Power law overlap of six uHF as a function of normalized Q exponent of $1/T^Q$ in a double logarithmic representation. The 'SC-PM' region identifies the spin correlated-paramagnetic phase and T_{BN} the temperature of the onset of the $C_{\mathrm{m}}/T|_{T\to 0}$ 'plateau' regime. See the text for references (Color figure online)

3 Thermodynamic Analysis of the $S_{\mathrm{m}}(T)$ Trajectories

3.1 Origin of the $C_{\mathrm{m}}/T|_{T\to 0}$ Upper Limit: Entropy Bottlenecks

Since these systems are inhibited to order magnetically because of their frustrated character, spin correlations develop remarkably by decreasing temperature within the 'SC-PM phase'. As a consequence, the density of magnetic excitations ($\propto C_{\mathrm{PM}}/T$) grows following a power law, as depicted in Fig. 4a for the exemplary system $YbCu_{4.3}Au_{0.7}$, that extrapolates to a mathematical singularity at $T = 0$. Therefore, a change of behavior is expected at finite temperature (hereafter T_{BN}) in order to escape such unphysical point. The question arises why this change of regime occurs at certain characteristic temperature T_{BN} and how is its value established. To attempt to answer these questions, one should take into account the relevance of the third law of thermodynamics at the $T \to 0$ limit.

In order to analyze how the third law (shortly expressed as $S_{\mathrm{m}}(T)|_{T\to 0} \geq 0$) intervenes in determining the ground state (GS) of these uHF, the $C_{\mathrm{m}}(T)/T$ dependence of the magnetically frustrated $YbCu_{4.3}Au_{0.7}$ [12] is chosen. In its pyrochlore-type structure, the Yb-magnetic moments are located in tetrahedral vertices inhibiting magnetic order due to a 3D geometric frustration. This property guarantees that no condensa-

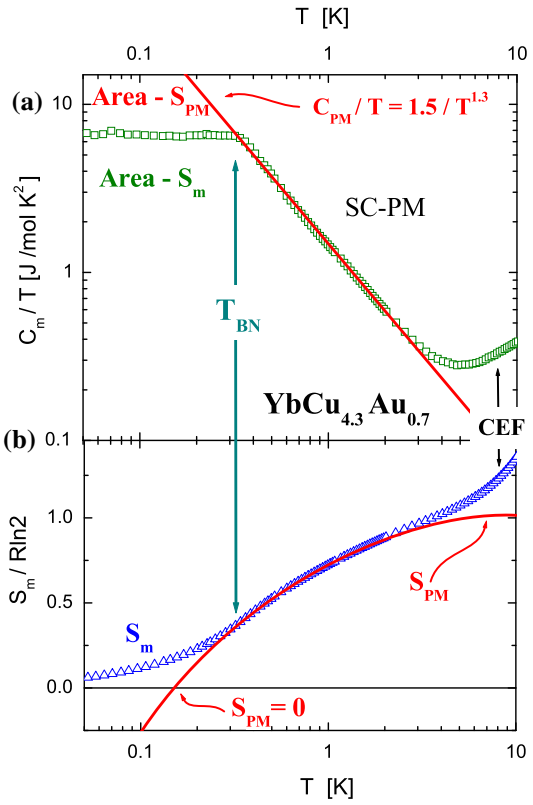

Fig. 4 **a** Comparison between measured $C_m(T)/T$ and fitted $C_{PM}/T|_{T>T_{BN}}$ dependencies (straight line) in double logarithmic representation for a magnetically frustrated system [12]. S_m and S_{PM} represent the areas from which respective entropies are evaluated. **b** Thermal dependencies of those entropies, showing how $S_{pm} \to 0$ at $T > 0$. The value of $S_{PM}(T \to \infty) = R\ln 2$ is taken as reference for the doublet GS. CEF indicates the excited crystal field levels contribution above about 3 K (Color figure online)

tion of degrees of freedom occurs by magnetic order induced via standard magnetic interactions. In fact, no traces of order were detected in this system below T_{BN} by spectroscopic measurements [21]. In Fig. 4a, one may appreciate that $C_m(T > T_{BN})/T$ increases obeying the power law dependence $\propto 1.5/T^{1.3}\,\mathrm{J/mol\,K^2}$ which, below $T_{BN} = 350\,\mathrm{mK}$, transforms into a 'plateau' with $C_m/T|_{T\to 0} \approx 6.5\,\mathrm{J/mol\,K^2}$. This plateau was obtained after subtracting the nuclear contribution of Yb atoms from the total measured specific heat [12].

The area label as Area-S_{PM} in Fig. 4a represents the entropy computed as $S_{PM} = \int 1.5/T^{1.3} \times \mathrm{d}T$ for a heuristic system which does not change its C_{PM}/T dependence at T_{BN} and clearly exceeds the 'Rln 2' physical limit for a doublet GS. On the contrary, the entropy extracted from the measurement as $S_m = \int C_m/T \times \mathrm{d}T$, represented by Area-$S_m$, reveals that the diverging increase of $C_m/T|_{T>T_{BN}}$ toward low temperature runs across an 'entropy bottleneck' (BN) [22] that compels it to change trajectory. This means that the change of $C_m(T)/T$ at $T = T_{BN}$ occurs because the system is constrained to not overcome the $S_m = R\ln 2$ value.

The comparison between $S_{PM}(T)$ and $S_m(T)$ trajectories is included in Fig. 4b. Since this analysis only involves doublet GS, the $R\ln 2$ upper limit at high temperature is taken as the reference value for $S_m(T)$. Notice that the contribution of the excited CEF levels to $S_m(T)$) only occurs above about $T = 3\,\mathrm{K}$. This comparison shows that

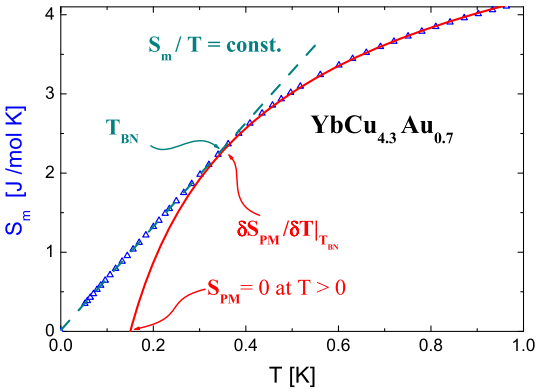

Fig. 5 Analysis of the thermodynamic condition producing the entropy deviation from the SC-PM trajectory. Continuous curve: $S_{\mathrm{PM}}(T)$, dashed line: $S_{\mathrm{m}}/T =$ constant (Color figure online)

both entropy trajectories clearly match within the $0.3 \geq T \geq 2\,\mathrm{K}$ range. However, while $S_{\mathrm{m}}(T < 0.3\,K)$ turns pointing to the expected $S_{\mathrm{m}}|_{T\to 0} = 0$ limit, $S_{\mathrm{PM}}(T)$ crosses the 'zero' value at finite temperature (at $T \approx 0.17\,\mathrm{K}$ in this case) and keeps decreasing into negative values. It is clear that below $T = T_{\mathrm{BN}}$ the third law imposes a change of trajectory to $S_{\mathrm{m}}(T)$, which departs from $S_{\mathrm{PM}}(T)$ in order to not overcome the physical limit of $S_{\mathrm{m}}|_{T\to 0} = 0$. A relevant aspect of this change in $S_{\mathrm{m}}(T)$ arises from the fact that it is not driven by magnetic interactions but by the thermodynamic constraint: $S_{\mathrm{m}}|_{T\to 0} \geq 0$.

3.2 Conditions to Deviate from the SC-PM Behavior

Once the origin of the change of regime was risen, one should trace the thermodynamic conditions able to split $S_{\mathrm{m}}(T)$ and $S_{\mathrm{PM}}(T)$ trajectories at $T = T_{\mathrm{BN}}$. For such a purpose we focus on $S_{\mathrm{m}}(T_{\mathrm{BN}})$ and $S_{\mathrm{PM}}(T_{\mathrm{BN}})$ coincidences. Looking at the same frustrated system $YbCu_{4.3}Au_{0.7}$, one may see in Fig. 5 that at T_{BN} the entropy derivative $\partial S_{\mathrm{m}}/\partial T$ ($= \partial S_{\mathrm{PM}}/\partial T$) coincides with the $S_{\mathrm{m}}(T < T_{\mathrm{BN}})/T$ ratio that extrapolates to $S_{\mathrm{m}}|_{T\to 0} = 0$. Then, taking into account that $\partial S_{\mathrm{m}}/\partial T \equiv C_{\mathrm{m}}/T$, one finds that $C_{\mathrm{m}}/T_{\mathrm{BN}} = S_{\mathrm{m}}/T_{\mathrm{BN}}$ and therefore $S_{\mathrm{m}} = C_{\mathrm{m}}$ at that temperature.

Since the specific heat is defined as $C_{\mathrm{m}} \equiv \partial E_{\mathrm{m}}/\partial T$, where E_{m} is the magnetic enthalpy, the $S_{\mathrm{m}} = C_{\mathrm{m}}$ equality can be written as: $S_{\mathrm{m}} - \partial E_{\mathrm{m}}/\partial T = 0$. This expression coincides with the Planck's potential: $\Phi = S - E/T$ [23] provided that $\partial E_{\mathrm{m}}/\partial T = E_{\mathrm{m}}/T$, which is the case of the so-called plateau regime of the uHF showing $C_{\mathrm{m}}/T|_{T\to 0} =$ const. That property fulfills the $\Phi = S_{\mathrm{m}} - E_{\mathrm{m}}/T = 0$ condition. Another relationship that characterizes this change if the regime can be extracted from $\partial S_{\mathrm{m}}/\partial T = S_{\mathrm{m}}/T$ writing $\partial S_{\mathrm{m}}/S_{\mathrm{m}} = \partial T/T$. This implies that, at $T = T_{\mathrm{BN}}$, the entropy and temperature (i.e., thermal energy) variation occurs with the same relative ratio, i. e. $\partial \ln S_{\mathrm{m}}/\partial \ln T = 1$.

3.3 Other Cases with Similar Thermal C_{PM}/T Dependencies

In order to recognize whether this 'entropy-bottleneck' effect only occurs in the uHF with a $C_{\mathrm{m}}/T|_{T\to 0}$ 'plateau' below T_{BN} or it is a general property, the same

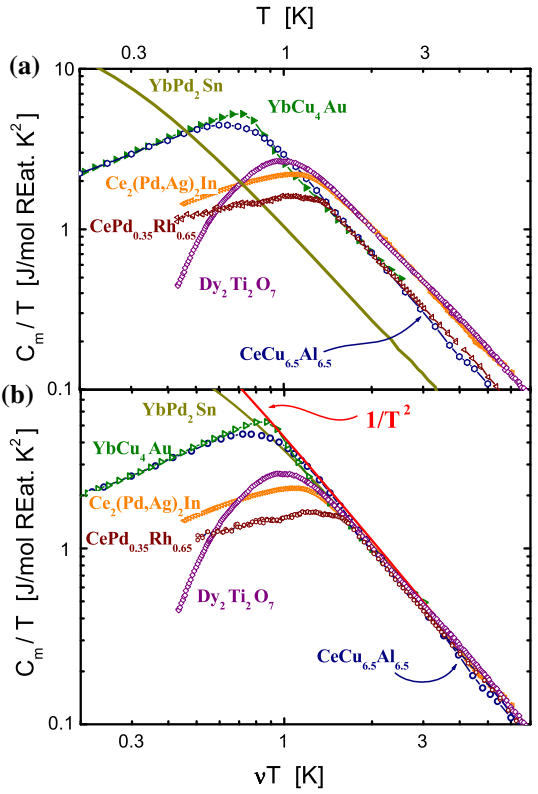

Fig. 6 **a** Compounds with $C_m(T)/T$ maxima at $T \approx 1$ K and the same power law dependence in their 'SC-PM' phases, see the text for references. Notice the double logarithmic representation and the mol-RE normalization to a single rare earth (RE) atom. **b** Same compounds scaled by normalizing their respective temperatures with a factor ν, taking $Dy_2Ti_2O_7$ [24] and $Ce_2(Pd_{0.5}Ag_{0.5})_2In$ as reference. A $1/T^2$ function is included to show the coincident dependence of these compounds (Color figure online)

analysis is applied to a number of compounds collected in Fig. 6a none of which show long range magnetic order. The figure contains some geometrically frustrated cases, like the 3D-pyrochlores $YbCu_4Au$ [25] and $Dy_2Ti_2O_7$ spin-ice [26] and the 2D $Ce_{2.15}(Pd_{0.5}Ag_{0.5})_{1.95}In_{0.9}$ [27], hereafter quoted as $Ce_2(Pd_{0.5}Ag_{0.5})_2In$ for simplicity, that shows on-plane triangular coordination between Ce-nearest-neighbors in a Mo_2B_2Fe-type structure. A striking feature observed in all the mentioned systems is the coincident power law dependence $C_m/T \propto 1/T^2$ in the respective 'SC-PM' phases.

To explore the ampleness of this peculiar dependence besides frustration phenomena, other set of compounds like: $YbPt_2Sn$ [11], $CeCu_{6.5}Al_{6.5}$ [28] and $CePd_{0.35}Rh_{0.65}$ single crystal [29] are included into this comparison (see Fig. 6a) because they show the same $C_m/T \propto 1/T^2$ dependence. Although the competition between the first (J_1) and second (J_2) neighbor exchange interactions may cause frustration in simple structures, the case of $CePd_{0.35}Rh_{0.65}$ seems to escape to that pattern because it was actually investigated in the context of a QC regime [30]. This supports one of the main points of the present analyses: the change in the $S_m(T)$ trajectory is due to thermodynamic constraints independently of the reason why magnetic order is inhibited. Coincidentally, the lack of magnetic order down to very low temperature provides the conditions for the *entropy-bottleneck* occurrence. However, these systems do not

show the uHF-plateau below T_{BN} because, once the entropy bottleneck conditions are reached, they access to some alternative minima of their free energy as evidenced by the decrease of their $C_m/T|_{T<T_{BN}}$.

As a consequence of their common power law dependence, the $C_{PM}/T|_{T>T_{BN}}$ results from these compounds can be normalized by simply scaling their density of excitations. Taking profit that all the systems included in Fig. 6a are properly described by the same heuristic formula $C_{PM}/T = D/(T^Q + E)$ [31], with $Q = 2 \pm 0.1$, the normalization of their respective D_ν coefficients as $D_\nu = \nu D$ collapses their $C_{PM}/T|_{T>T_{BN}}$ curves into a unique one presented in Fig. 6b. For such a purpose, the coincident $D = 4.5$ J/mol RE. Value of $Dy_2Ti_2O_7$ and $Ce_2(Pd_{0.5}Ag_{0.5})_2In$ is taken as a (arbitrary) reference. Notably, these two systems also coincide in their $E = 0.3\,K^2$ parameter [27].

In this comparison, the $C_m(T)/T$ properties of $YbPt_2Sn$ merit some comment because it coincides with some characteristics of this group but differs from others. Together with its homologous $YbPt_2In$ [11], its $C_{PM}(T)/T \propto 1/T^2$ dependence coincides with the common $Q \approx 2$ exponent of other compounds despite showing the lowest temperature maximum of $C_m(T)/T$. This feature supports the fact that the underlying mechanism responsible for the entropy-bottlenecks formation does not depend of an energy scale but reflect a general thermodynamic property. Besides that, these $YbPt_2X$ compounds show that the ≈ 7 J/mol K^2 value observed in the 'plateau' group is not an upper limit for $C_m/T|_{T\to 0}$ but a characteristic of those uHF.

The coincident $Q \approx 2$ exponent clearly suggests that some common physics underlies in their 'SC-PM' behavior. Although power law dependencies for C_m/T were reported in model predictions, those exponents used to be much smaller [1] than the ones observed in the systems at hand (i.e., $Q \ll 1$). Nevertheless, a $Q = 2$ exponent was reported [32] to describe the thermal properties of Kondo-type systems assuming a uniform distribution of T_K between 0 and a cut-off energy with a $C_m/T \propto 1/(T^2+T_K^2)$ dependence. In the present context, T_K may represent the energy scale that characterizes a spin-liquid (SL) scenario, making this function to fit so nicely the reported measurements.

Interestingly, all systems included in Fig. 6 exhibit a $C_m/T \propto T$ dependence below their maxima, with the exception of $Dy_2Ti_2O_7$. This difference may arise from the intermetallic nature of the Ce- and Yb-based compounds that may favor the typical RKKY interaction instead of other (Oxygen mediated) exchange mechanisms. This coincidence was the main reason for the inclusion of $Dy_2Ti_2O_7$ into the comparison presented in Fig. 6 because it indicates that the strong increase in the density of excitations, approaching the maximum of $C_m(T)/T$ from high temperature, is dominated by the frustrated nature of the magnetic interactions not by the nature of those interactions. Nevertheless, the difference is clearly observed below the $C_m(T)/T$ maximum.

3.4 Comparison Between Different Entropy Behaviors

Regarding the thermal dependence of the entropy, the same discussion performed in Fig. 4 about the change of trajectory at T_{BN} can be applied to these compounds, see Fig. 7a. Two representative cases are included in the figure: $Ce_2(Pd_{0.5}Ag_{0.5})_2In$

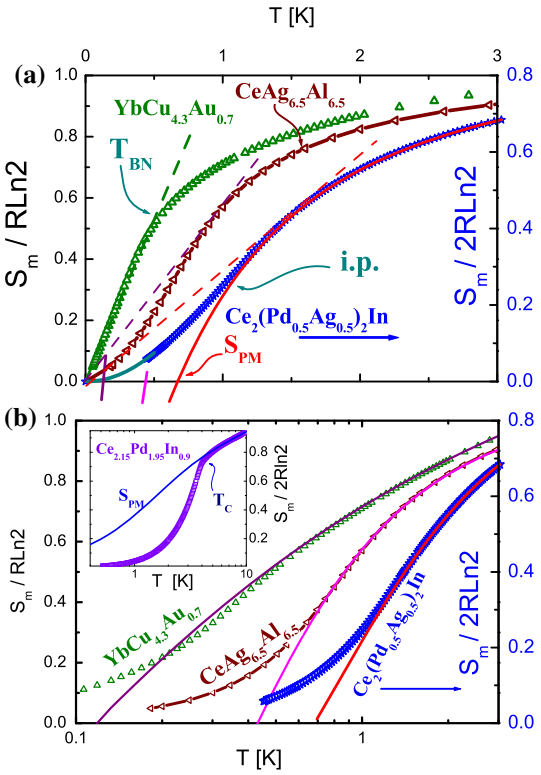

Fig. 7 **a** $S_m(T)$ dependencies of three compounds showing their respective $S_{PM} = 0$ extrapolations at $T > 0$ and S_m/T (dashed) lines defining respective T_{BN}. The $S_m(T)$ inflexion point in one of the systems is indicated as 'i.p.'. **b** Same entropy dependencies in a log(T/K) representation compared with that of a standard ferromagnetic compound (see the inset) (Color figure online)

and $CeCu_{6.5}Al_{6.5}$, and compared with $YbCu_{4.3}Au_{0.7}$ as a member of the 'plateau' group. Each $S_{PM}(T)$ dependence is computed as $S_{PM} = \int C_{PM}/T \times dT$, with respective $C_{PM}(T > T_{BN})/T = 1.46/T^{1.3}$ J/mol K^2 for $YbCu_{4.3}Au_{0.7}$, $= 9.1/(T^2 + 0.35)$ J/mol K^2 for $Ce_2(Pd_{0.5}Ag_{0.5})_2In$ and $= 3/T^2$ for $CeCu_{6.5}Al_{6.5}$. As it can be seen, all these $S_{PM}(T)$ trajectories cross the $S_m = 0$ axis at finite temperature because $S_{PM}|_{T\to 0}$ extrapolates to the unphysical value $S_{PM}|_{T=0} < 0$ if the reference value of Rln 2 is taken as reference for the doublet GS of these compounds.

Focusing to the actual value of S_m at T_{BN}, it is evident from Fig. 7a that $S_m(T_{BN}) \approx 1/2R \ln 2$. Within a significantly low dispersion, this observation includes the $CePt_2X$ compounds [11] and frustrated systems like $Ce_2(Pd_{0.5}Ag_{0.5})_2In$ and $Dy_2Ti_2O_7$. Interestingly, the $Dy_2Ti_2O_7$ spin-ice fits better into this systematic once the Pauling's residual entropy $S_0 = (1/2)R \ln(3/2)$ [33] is included into the 'total' $S_{tot} = S_m + S_0$.

In Fig. 7b, the same comparison is shown in a 'log(T/K)' representation in order to better distinguish the detachment between measured $S_m(T)$ and computed $S_{PM}(T)$ below $T = T_{BN}$. Interestingly, in $YbCu_{4.3}Au_{0.7}$ the $S_m(T)$ trajectory is slightly lower than the extrapolated $S_{PM}(T)$ one around T_{BN}. This looks like as a reminiscence of a second-order transition, but a small deviation fits into the scale of eventual composition inhomogeneities, e.g., at the surface of these poly-crystalline samples. The case of the ferromagnet $Ce_{2.15}Pd_{1.95}In_{0.9}$ [34] is included as an inset of this figure for comparison. This magnetically ordered compound was selected because it shows

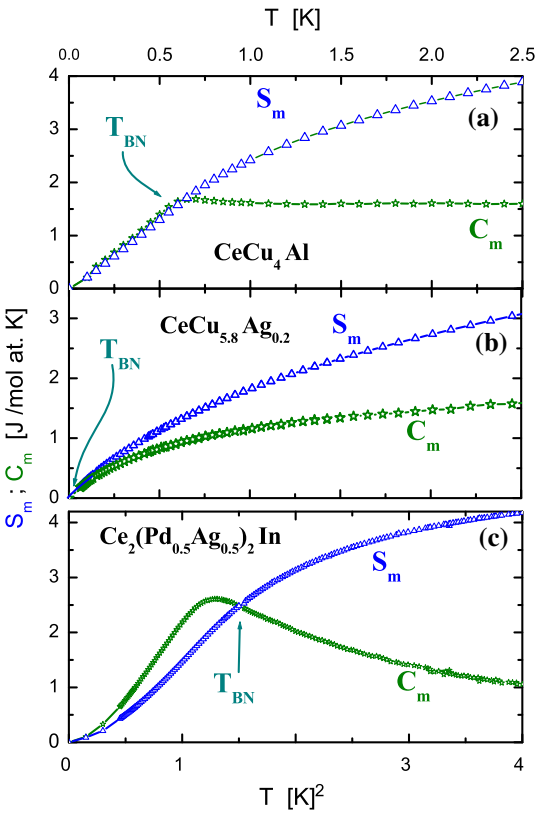

Fig. 8 Comparison of $S_m(T)$ and $C_m(T)$ dependencies for three different types of GS: **a** a 'plateau' type with $T_{BN} \approx 0.6$ K, data after [36], **b** the case of a NFL [37] where $\Phi(T) = 0$ occurs at $T_{BN} = 0$, and **c** a 2D frustrated system showing a $C_m(T)/T_{max}$ at ≈ 1 K, data after [27] (Color figure online)

a well-defined $C_m(T_C)$ jump at relatively low temperature, $T_C = 4.1$ K, among other Ce-based compounds. It is evident that in this case the corresponding paramagnetic $S_{PM}(T > T_C)$ extrapolation below T_C is well above the measured $S_m(T < T_C)$ values, in clear contrast with the not ordered compounds that upturn with respect to S_{PM} at $T \approx T_{BN}$. One should also notice that, while the discontinuity in the $\partial S_m/\partial T$ slope implies a C_m/T jump at $T = T_C$, the inflection of $S_m(T)$ around T_{BN} (labeled 'i.p.' in Fig. 7a) is associated with a discontinuity in the second ($\partial^2 S_m/\partial T^2$) derivative. This corresponds to a jump in the specific heat derivative (i.e., $\partial C_m/\partial T$) like in a third-order-type transition [35].

To check the applicability of the $C_m = S_m$ equality in a wider range of behaviors, it is illustrative to compare the $C_m(T)$ and $S_m(T)$ dependencies in other systems that do not order magnetically but having their GS of different nature. In Fig. 8a, the stoichiometric compound $CeCu_4Al$ with a $T_{BN} \approx 0.6$ K, [36] is included as another example showing $C_m/T|_{T\to 0}$ constant and hence a coincident $C_m(T)$ and $S_m(T)$ below T_{BN}. Interestingly, as it is depicted in Fig. 8b the NFL $CeCu_{5.8}Ag_{0.2}$ [37] reaches the $C_m(T) = S_m(T)$ equality at $T = 0$ revealing that $T_{BN} = 0$ for these systems. Due to their $C_m \propto -T \times \ln(T/T_0)$ dependencies the $C_m(T) - S_m(T)$ difference is expected to increase linearly with temperature. $CeCu_{5.8}Ag_{0.2}$ was chosen as a NFL

exemplary system because it shows the largest measured value $C_m/T = 3\,\mathrm{J/mol\,K^2}$ at $T = 60\,\mathrm{mK}$ included in Fig. 2. In spite of this, it does not reach the values of uHF even at $T \to 0$ because it shows a slight downwards deviation that extrapolates to $C_m/T|_{T=0} < 4\,\mathrm{J/mol\,K^2}$. Figure 8c includes an example of a 2D frustrated system $Ce_2(Pd_{0.5}Ag_{0.5})In$ [27]. As expected from the analysis performed in Fig. 7a, the $C_m = S_m$ equality occurs where $C_m(T)/T$ deviates from the 'SC-PM' regime described by the $\propto 1/T^2$ dependence. This temperature is close but not exactly at the maximum of $C_m(T)$. A replica of this behavior is obtained for the $Dy_2Ti_2O_7$ spin-ice. This comparison supports the conclusion that the entropy bottleneck is a general effect occurring in systems not able to reach magnetic order.

4 Thermodynamic Behavior at $T \leq T_{BN}$

In order to gain insight into the behavior of these systems, one should focus on the two main questions arising from the observed phenomenology that mostly concerns the change of regime at $T = T_{BN}$ and the nature of the GS beyond the entropy bottleneck. Although the usual Kondo scenario, able to explain the lack of magnetic order applies, e.g., to $CePd_{0.35}Rh_{0.65}$,[1] in the range of temperatures where the entropy bottlenecks occur ($T_{BN} \leq 1\,\mathrm{K}$), also quantum fluctuations may play an important role in the thermodynamic equilibrium because they may overcome thermal fluctuations even far away from a quantum critical point [31].

Recent theoretic descriptions of phase diagrams for magnetically frustrated systems include the possibility of a continuous transition between a small paramagnetic Fermi surface (P_S), without relevant Kondo screening, to a large one (P_L) characteristic of FL behavior [38,39]. These models seem to apply to the 'plateau' group that, after behaving as a localized '$4f$' electron lattice (P_S type), they turn into a constant $C_m/T|_{T\to 0}$ dependence at $T = T_{BN}$ (P_L type). Similarly, the family of compounds showing a $C_m(T)/T$ maximum at $T \approx 1\,\mathrm{K}$ could be included in the case where the system runs between a P_S phase and an incipient spin-density-wave state. It is worth noting that these phase diagrams are mostly focused into specific frustrated materials like, e. g., those showing Shastry-Sutherland lattices formation which are formulated as a function of two competing interactions J_1/J_2. However, the systems included in Figs. 3b and 6 extend this framework to purely geometrically frustrated ones, like those represented by the 2D (triangular) $Ce_2(Pd_{0.5}Ag_{0.5})_2In$ or 3D (tetrahedral) $YbCu_4Ni$ or $Dy_2Ti_2O_7$ lattices.

4.1 Characteristics of the T_{BN} Transition

In Fig. 9a, the $C_m(T)$ dependence of other three systems is presented to show the effect of the entropy bottleneck through an alternative perspective. From the $C_m(T > T_{BN}) \approx$ const. behavior, it is evident that they would extrapolate to a non-physical

[1] Notice that $CePd_{0.35}Rh_{0.65}$, as an example of QC behavior, is included to show that the change in the $S_m(T)$ trajectory is due to thermodynamic constraints, independently of the cause of the lack of magnetic order

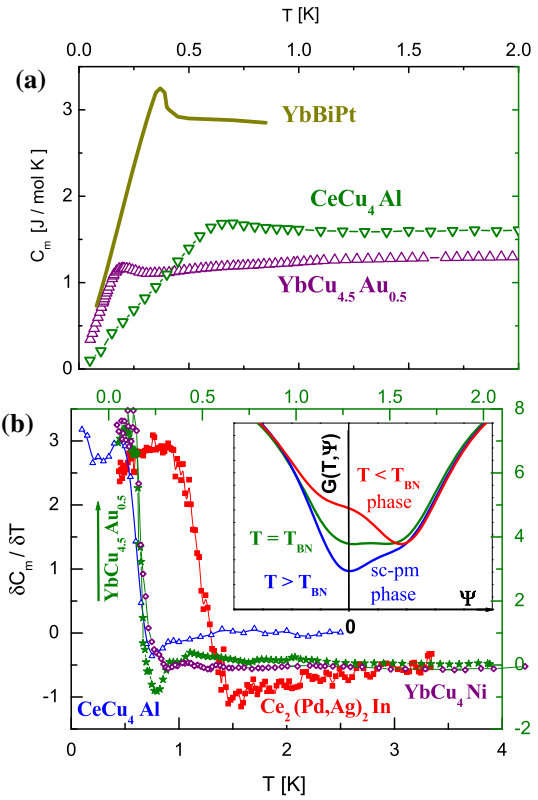

Fig. 9 **a** Three illustrative cases: YbBiPt [18], $CeCu_4Al$ [36] and Yb $Cu_{4.5}Au_{0.5}$ [12] (right and upper axes), showing how $C_m(T)$ extrapolates to $C_m \neq 0|_{T\to 0}$ before the entropy bottleneck is reached. **b** $\partial C_m/\partial T$ derivative of some studied compounds showing a discontinuity at $T = T_{BN}$. Upper and right axes correspond to $YbCu_{4.5}Au_{0.5}$ data. Inset: isothermal $G(\Psi)$ representations for three different temperatures including a broad minimum at $T = T_{BN}$, after [40] (Color figure online)

$C_m \neq 0$ at $T = 0$ unless a change trajectory occurs. Like in the discussion of Fig. 7a, the small jump at T_{BN} can be likely attributed to composition inhomogeneities at grains-surface of these poly-crystalline samples.

Since the change in regime occurs without undergoing a typical mean field $C_m(T)$ jump, the following scenario can be proposed: the minimum of the free energy of the SC-PM phase (G_{PM}) blurs out at T_{BN} and the system is compelled to slide into any other energetically accessible $G(T)$-minimum. This description is schematically depicted in the inset of Fig. 9b [40] as a $G(\Psi)$ dependence on the order parameter Ψ at different temperatures. This continuous creep along the $G(\Psi, T)$ surface is related to a higher-order discontinuity of the $G(T)$ derivative, i.e., $\partial G^3/\partial^3 T$, that emerges as the mentioned 'inflection point' in Fig. 7a and as a discontinuity in $\partial C_m/\partial T$. These features correspond to third-order-type transitions according to thermodynamic criteria [35]. In comparison, the exemplary case of second-order FM transition included the inset of Fig. 7b shows a well-defined $\Delta C_m(T_C)$ jump because an 'order parameter' $\Psi(T < T_C)$ develops below the transition, associated with the $\partial S_m/\partial T$ discontinuity.

One should take into account that, while interactions define different possible magnetic configurations, thermodynamics 'recognizes' which one has the lowest energy. In other words, magnetic interactions and thermodynamics constraints act intertwined to define the GS of real system. In the case that interactions are not able to define any

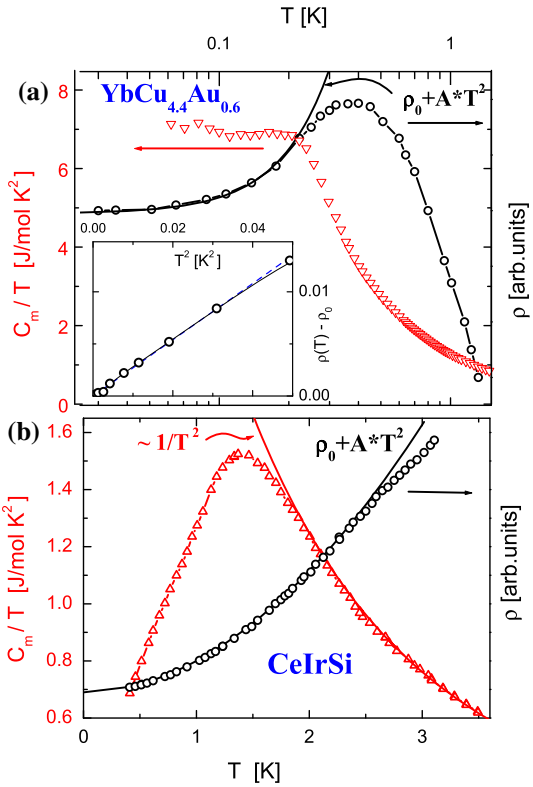

Fig. 10 Continuous formation of a coherent GS indicted by electrical resistivity (fitted as $\rho_0 + AT^2$) of systems belonging to: **a** the 'plateau' group, with data after [12,41] and **b** to one of those with the C_m/T maximum at $T_{BN} \approx 1$ K, after [45] (Color figure online)

magnetic configuration with lower energy than that of the frustrated (paramagnetic) one, thermodynamic parameters are anyway inhibited from transgressing the Nersnt postulate.

4.2 Nature of the Ground State Beyond the Entropy Bottleneck

Despite the reduced experimental data on physical properties at the mK range some relevant features can be recognized from the available information. Starting with one member of the 'plateau' group, $YbCu_{4.4}Au_{0.6}$, one finds that the absence of magnetic order was confirmed down to 20 mK from μSR and NQR measurements [21], i.e., far below the $T_{BN} = 300$ milikelvin temperature. Coincidentally, the formation of a coherent GS is observed in $\rho(T)$ [41], see Fig. 10a, with the onset of coherence around T_{BN}. As shown in the inset of that figure $\rho(T) \approx AT^2$, and therefore this behavior might be associated with the formation of a FL or a SL state. However, $C_m(T)/T$ does not follow the thermal evolution for a standard FL because it shows a change of regime from the 'plateau' at T_{BN} to a power low dependence instead of a continuous deviation from a constant $C_m(T \to 0)/T$ value without any discontinuity in its slope.

Interestingly, $YbCu_{4.4}Au_{0.6}$ shows a $\rho(T)$ maximum at $T \approx 0.5$ K like other components of the 'plateau' group, e.g., $YbCo_2Zn_{20}$ [42], that can be associated

with a Kondo or spin fluctuation energy scales. Also the magnetic susceptibility (χ) of $YbCo_2Zn_{20}$ confirms the lack of magnetic order below T_{BN} because its $\chi(T)$ dependence simply shows a broad maximum at $T \approx 300\,\text{mK}$ [43]. The absence of magnetic order was also remarked in YbBiPt [18], with a considerably small T_K and a monotonous decrease of $\rho(T)$. Similar, $\rho(T)$ coherence effects are observed in $PrInAg_2$ around $T_{BN} \approx 250\,\text{mK}$ [17]. Notably, the doublet GS of this compounds is not a Kramer-type doublet because of the integer $J = 4$ total angular moment of Pr. This indicates that the notion of an entropy bottleneck is irrelevant for the physical nature of the GS.

Concerning the family of compounds showing a $C_m(T)/T$ anomaly centered at $T_{BN} \approx 1\,\text{K}$, the absence of magnetic order was confirmed in the exemplary spin-ice $Dy_2Ti_2O_7$ [44] by transverse-field μSR experiments as expected. A coherent GS formation is also supported by $\rho(T)$ measurements in CeIrSi [45], where Ce-atoms coordination provides the geometrical condition for magnetic frustration. In this compound, $\rho(T)$ obeys a $\rho = \rho_0 + A \times T^2$ dependence for $T \leq 2.4\,\text{K}$ which reveals the coherent electronic scattering, see Fig. 10b. This range of temperature fully covers respective $C_m(T)/T$ and $\chi(T)$ anomalies around $T_{BN} \approx 1.4\,\text{K}$ indicating that the coherence sets on clearly above those maxima.

From these experimental evidences, one may conclude that the GS of these compounds behaves more likely as FL or SL, without relevant long range J_R-like interactions that justifies the observed coherence, and that magnetic interactions can be discarded as the origin of the $T \approx T_{BN}$ maxima. Moreover, taking into account that this phenomenon occurs within the mK range of temperature, dominated by quantum fluctuations, also eventual tunneling mechanisms between states of equivalent energy might act as a hopping mechanism. In such a case, the formation of a very narrow band associated with the extremely high values of $C_m/T|_{T\to 0}$ value may arise. However, to our knowledge, there is no specific experimental information in the literature for this scenario nor for $C_m(T)$, $\rho(T)$ or $\chi(T)$ of SL systems.

4.3 Thermal Dependence of the Entropy at $T \to 0$

Despite the leafy literature devoted to the $S_m|_{T\to 0} \geq 0$ postulate, there is scarce information about how $S_m(T)$, i.e., its derivatives, approaches $T = 0$ [46]. Although the unattainability of that limit prevents any experimental approximation, the present knowledge of the $S_m(T)$ behavior of non-ordered Ce- and Yb-based compounds allows to explore that field from a phenomenological point of view. This topic becomes relevant concerning the efficiency of new cryo-materials for adiabatic demagnetization because it depends on temperature and magnetic field (H) variations as $dS(T, H) = (\partial S/\partial T)|_H dT + (\partial S/\partial H)|_T dH$ that, in the adiabatic branch, equals zero.

Some interesting features can be extracted from the analysis of the possible trajectories of $S_m|_{T\to 0}$, schematically drown in Fig. 11a and formerly discussed in Ref. [47]. The three possible curvatures presented in the figure can be classified according to their second thermal derivatives, $\partial^2 S_m/\partial T^2$: (i) the positive ($> 0$) curvature corresponds to systems reaching a standard long range order, which is represented by the FM compound $Ce_{2.15}Pd_{1.95}In_{0.9}$ introduced in the inset of Fig. 7b, (ii) the zero curva-

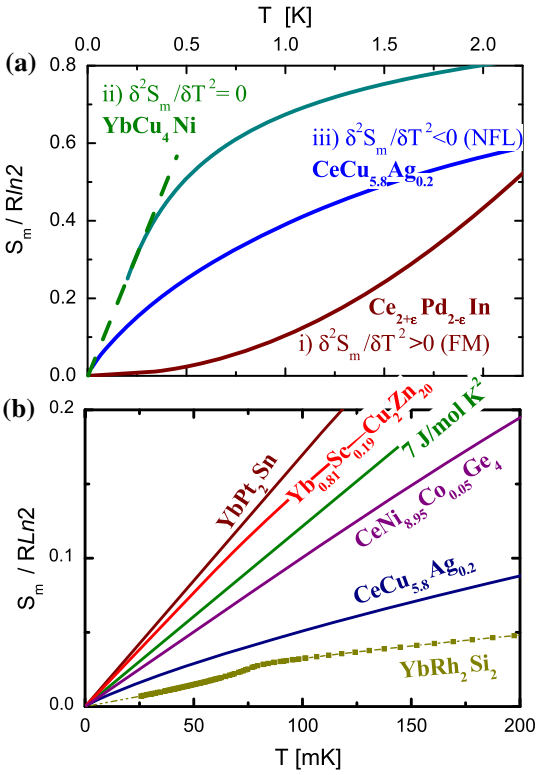

Fig. 11 **a** Three different ways for $S_m|_{T\to 0}$ according to its second derivative $\partial^2 S_m/\partial T^2$. **b** Comparison of the $S_m|_{T\to 0}$ among real systems in the mK range. Label '7J/molK^2' represents the members of the 'plateau' group. See the text for references (Color figure online)

ture ($\partial^2 S_m/\partial T^2 = 0$ or constant $C_m/T|_{T\to 0}$) identifies the members of the 'plateau' group and any system forming an electronic band like, e.g., the FL. (iii) The negative curvature (< 0) is characteristic of uHF or NFL systems that do not reach an ordered GS. As it was discussed, uHF are compelled to modify their $S_m(T)$ trajectory at T_{BN} to deviate from their divergent $C_m/T|_{T\to 0}$, like the exemplary case of $YbCu_4Ni$ included in Fig. 11a.

The lowest temperature $\partial^2 S_m/\partial T^2|_{T\to 0} < 0$ curvature is expected for NFL compounds because their $C_m \propto -T \times \ln(T/T_0)$ dependence corresponds to a $T_{BN} = 0$, like in the case of $(Yb_{0.81}Sc_{0.19})Co_2Zn_{20}$ [20] and $Ce(Ni_{8.95}Co_{0.05})Ge_4$ [48]. In the case of NFL, the extended energy range of magnetic excitations produces a moderate increase of the entropy $S_m(T) \propto T - T \times ln(T/T_0)$ in the mK range allowing the closest approach to $\partial^2 S_m/\partial T^2|_{T=0} < 0$, shifting the entropy-bottleneck conditions down to $T = 0$. These and other Yb- and Ce-based systems are compared in Fig. 11b within the $T < 200$ mK range. The intensively studied $YbRh_2Si_2$ compound [49] is also included for comparison to a case of a NFL-like behavior that orders at 80 mK. In all cases, the measured $C_m(T)/T$ data are extrapolated to $T = 0$ with the same value of the lowest temperature measured point to partially account for the entropy increase below about 50 mK.

It becomes evident that, with the exception of $(Yb_{0.81}Sc_{0.19})Co_2Zn_{20}$ and $Ce(Ni_{8.95}Co_{0.05})Ge_4$ alloys, most of NFL are not suitable compounds for adiabatic

magnetization processes. A common feature of these two exceptions is the fact that respective NFL behaviors are obtained introducing atomic disorder by alloying stoichiometric uHF compounds. The complementary requirement for an appropriate cryo-material is to have a strong $\partial S/\partial H)|_T$ variation, as it was observed in $YbPt_2In$ [4] and $(Yb_{0.81}Sc_{0.19})Co_2Zn_{20}$ [20]. Once again classical NFL do not show strong $\partial S/\partial H)|_T$ variations.

5 Conclusions

Along this work, it was shown how the absence of magnetic order, inhibiting magnetic degrees of freedom to condensate into a singlet GS, can be profited to investigate the effects of the third law of thermodynamics in real materials. It was analyzed how the enhanced paramagnetic correlations strongly increase the density of low-energy excitations inducing the formation of uHF-GS. Apart from the quantitative differences of $C_m/T|_{T\to 0}$ in uHF and NFL, respective power law and logarithmic thermal dependencies testify their distinct physical nature.

The divergent increase of the density of excitations collides with the limited amount of the available paramagnetic degrees of freedom (Rln 2 for a doublet GS) producing an entropy bottleneck which modifies the $S_m(T)$ trajectory. Such a 'bottleneck' occurs in these systems because they are not able to access an ordered state when approaching the exhaustion of their degrees of freedom. Since this change in the $S_m(T)$ trajectory is not driven by standard magnetic interactions but by thermodynamic constraints, this crossover occurs through a continuous transition of third-order character. The temperature at which the entropy bottleneck occurs was found to be associated with the $S_m = C_m$ equality.

Notably, among the compounds showing a constant $C_m/T|_{T\to 0}$ a nearly coincident value $\approx 7 \pm 0.7$ J/mol K^2 is detected. Despite the dispersion observed in the T_{BN} values of these compounds, the convergent value of $C_m/T|_{T\to 0}$ seems to be a characteristic property which identifies the 'plateau' group. Whether this specific value has an underlying physical origin remains an open question. Besides that, the spin fluctuation regime observed in $\rho(T \leq T_{BM})$ suggests a sort of FL or eventual SL behavior below that temperature. In standard FL, constant $C_m/T|_{T\to 0}$ and $\rho(T)$ coherence are related to narrow electron bands, that in the present scenario could be even associated with quantum tunneling mechanisms connecting levels of similar energy. This possibility certainly requires to be backed by microscopic investigations.

These systems also allow to perform an empirical approach to the study of the entropy derivatives, showing that negative curvature ($\partial^2 S_m/\partial T^2 < 0$) has the best physical representation in NFL compounds, whose logarithmic dependencies of $S_m(T)$ and $C_m(T)$ place the $S_m = C_m$ equality at $T = 0$. Apart from their NFL or uHF character, a relevant field dependence of S_m at the mK range, required for adiabatic demagnetization purposes, is only observed in very few uHF and the NFL induced by alloying a uHF compound.

Acknowledgements The author is grateful to I. Curlik, M. Giovannini, T. Gruner, M. Deppe, E. Bauer, H. Michor, M. Reiffers, E.-W. Scheidt, A. Strydom and I. Zeiringer for allowing to access to original

experimental results. This work was partially supported by Projects: PIP-2014 Nr. 112-2013-0100576 of CONICET and SECyT 06/C520 of Univ. of Cuyo (Arg.).

References

1. G.R. Stewart, Rev. Mod. Phys. **73**, 797 (2001)
2. H. Löhneysen, A. Rosch, M. Vojta, P. Wöfle, Rev. Mod. Phys. **79**, 1015 (2007)
3. S.A. Kivelson, A. Muramatsu, New J. Phys. http://iopscience.iop.org/journal/1367-2630/page/. Focus on Quantum Spin Liquids
4. D. Jang, T. Gruner, A. Steppke, K. Mistsumoto, C. Geibel, M. Brando, Nat. Commun. **6**, 8680 (2015). https://doi.org/10.1038/ncomms9680
5. S. Doniach, Physica B & C **91**, 231 (1977)
6. M. Lavagna, C. Lacroix, M. Cyrot, Phys. Lett. **90A**, 210 (1982)
7. M. Lavagna, C. Lacroix, M. Cyrot, J. Phys. F **13A**, 1007 (1983)
8. T. Vojta, Ann. Phys. **9**, 403–440 (2000)
9. J.G. Sereni, Handbook on the physics and chemistry of rare earths, in *Low Temperature Specific Heat of Cerium Compounds, Ch. 98*, vol. 15, ed. by K.A. Cschneidner Jr., L. Eyring (elsevier Science Publishers B. V., Amsterdam, 1991), p. 1
10. C. Gold, M. Uffinger, M. Herzinger, G. Eickerling, W. Scherer, H. Michor, E.-W. Scheidt, J. Alloys Compd. **523**, 61 (2012)
11. T. Gruner, D. Jang, A. Steppke, M. Brando, F. Ritter, C. Krellner, C. Geibel, J. Phys. Condens. Matter **26**, 485002 (2014)
12. I. Curlik, M. Giovannini, J.G. Sereni, M. Zapotokova, S. Gabani, M. Reiffers, Phys. Rev. B **90**, 224409 (2014)
13. A. Amato, D. Jaccard, J. Flouquet, E. Lapierre, J.L. Tholence, R.A. Fisher, S.E. Lacy, J.A. Olsen, N.E. Phillips, J. Low Temp. Phys. **68**, 371 (1987)
14. See Ref. [1] and G.R. Stewart, Rev. Mod. Phys. **78**, 743 (2006)
15. J.G. Sereni, C. Geibel, M. G-Berisso, P. Hellmann, O. Trovarelli, F. Steglich, Phys. B **230–232**, 580 (1997)
16. A.M. Strydom, University of Johannesburg, South Africa, Private Communication (2016)
17. A. Yatskar, W.P. Beyermann, R. Movshovich, P.C. Canfield, Phys. Rev. Lett. **77**, 3637 (1996)
18. Z. Fisk, P.C. Canfield, W.P. Beyermann, J.D. Thompson, M.F. Hundley, H.R. Ott, E. Felder, M.B. Maple, M.A. Lopez de la Torre, P. Visani, C.L. Seamanet, Phys. Rev. Lett. **67**, 3310 (1991)
19. M.S. Torikachvili, S. Jia, E.D. Mun, S.T. Hannahs, R.C. Black, W.K. Neils, D. Martien, S.L. Budko, P.C. Canfield, PNAS **104**, 9960 (2007)
20. Y. Tokiwa, B. Piening, H.S. Jeevan, S.L. Budko, P.C. Canfield, P. Gegenwart, Sci. Adv. **2**, e1600835 (2016)
21. P. Carretta, R. Pasero, M. Giovannini, C. Baines, Phys. Rev. B **79**, 020401(R) (2009)
22. J.G. Sereni, in *Magnetic Systems: Specific Heat*, ed. by S. Hashmi (editor-in-chief), Materials science and materials engineering. (Elsevier, Oxford, 2016), p. 1–13; ISBN:978-0-12-803581-8
23. M. Planck, *Treatise on Thermodynamics* (Dover Publications Inc, New York, 1926)
24. Unpublished results obtained from a single-crystal sample provided by S. Grigera, Universidad Nacional de La Plata, Argentina (2008)
25. M. Galli, E. Bauer, St Berger, Ch. Dusek, M. Della Mea, H. Michor, D. Kaczorowski, E.W. Scheidt, F. Marabelli, Physica B **312–313**, 489 (2002)
26. Z. Hiroi, K. Matsuhira, M. Ogata, J. Phys. Soc. Jpn. **72**, 304545 (2003)
27. J.G. Sereni, M. Giovannini, M. Gómez Berisso, F. Gastaldo, J. Phys. Condens. Matter **28**, 475601 (2016)
28. U. Rauchschwalbe, U. Gottwick, U. Ahlheim, H.M. Mayer, F. Steglich, J. Less Commun. Met. **111**, 265 (1985)
29. S. Hartmann, M. Deppe, N. Oeshler, N. Caroca Canales, J.G. Sereni, C. Geibel, J. Optoelectron. Adv. Mater. **10**, 1607 (2008)
30. J.G. Sereni, T. Westerkamp, R. Küchler, N. Caroca-Canales, P. Gegenwart, C. Geibel, Phys. Rev. B **75**, 024432 (2007)
31. J.G. Sereni, J. Low Temp. Phys. **149**, 179 (2007)
32. A.J. Schofield, Contemp. Phys. **40**, 95 (1999)

33. A.P. Ramirez, A. Hayashi, R.J. Cava, R. Siddharthan, B.S. Shastry, Nature **399**, 333 (1999)
34. J.G. Sereni, M. Giovannini, M. G-Berisso, A. Saccone, Phys. Rev. B **83**, 064419 (2011)
35. A.B. Pippard, *Elements of Classical Thermodynamics* (Cambridge University Press, Cambridge, 1964)
36. E. Bauer, Adv. Phys. **40**, 417 (1991)
37. E.-W. Scheidt, D. Maurer, A. Weber, T. Götzfried, K. Heuser, S. Kehrein, R. Tidecks, Physica B **321**, 133 (2002)
38. Q. Si, Phys. Status Solidi B **247**, 476 (2010)
39. P. Coleman, A.H. Nevidomskyy, J. Low Temp. Phys. **161**, 182–202 (2010)
40. J.G. Sereni, J. Low Temp. Phys. **179**, 126 (2015)
41. K. Yoshimura, T. Kawabata, N. Sato, N. Tsujii, T. Terashima, C. Terakura, G. Kido, K. Kosuge, J. Alloys Compd. **317318**, 465 (2001)
42. T. Kong, V. Taufour, S.L. Budko, P.C. Canfield, Phys. Rev. B **95**, 155103 (2017)
43. T. Takeuchi, M. Ohya, S. Yoshiuchi, M. Matsushita, F. Honda, R. Settai, Y. Onuki, J. Phys. Conf. Ser. **273**, 012059 (2011)
44. S.R. Dunsiger, A.A. Aczel, C. Arguello, H. Dabkowska, A. Dabkowski, M.-H. Du, T. Goko, B. Javanparast, T. Lin, F.L. Ning, H.M.L. Noad, D.J. Singh, T.J. Williams, Y.J. Uemura, M.J.P. Gingras, G.M. Luke, Phys. Rev. Lett. **107**, 207207 (2011)
45. F. Kneidinge, Ph.D. Thesis, Technische Universität Wien, unpublished (2013)
46. J.P. Abriata, D.E. Laughlin, Prog. Mater. Sci. **49**, 367 (2004)
47. J.G. Sereni, Philos. Mag. **93**, 409 (2013)
48. L. Peyker, C. Gold, W. Scherer, H. Michor, E.-W. Scheidt, J. Phys. Conf. Ser. **273**, 012049 (2010)
49. C. Krellner, S. Hartmann, A. Pikul, N. Oeschler, J.G. Donath, C. Geible, F. Steglich, J. Wosnitza, Phys. Rev. Lett. **102**, 196402 (2009)